NUMERICAL PARAMETRIC STUDY ON CO2 CAPTURE BY INDIRECT THERMAL SWING ADSORPTION

Marc Clausse, Jérôme Merel, Francis Meunier

NUMERICAL PARAMETRIC STUDY ON CO_2 CAPTURE BY INDIRECT THERMAL SWING ADSORPTION

Marc CLAUSSE*, Jérôme MEREL and Francis MEUNIER

Laboratoire de Génie des Procédés pour l'Environnement, l'Energie et la Santé

(LGP2ES - EA 21), Cnam

Dept. ICENER, case 2D3P20, 292 rue Saint-Martin, 75141 Paris Cedex 03, France

* Tel: +33 1.58.80.85.49, Fax: +33 1.40.27.20.47, E-mail: marc.clausse@cnam.fr

ABSTRACT

Post-combustion CO_2 capture remains one of the most-challenging issue to lower CO_2 emissions of existing power plants or heavy industry installations because of strong economy and energy efficiency aspects. The major issue comes from CO_2 dilution (4% for NGCC and 14% for PC) and the high flow rates to be treated. Furthermore, CO_2 purity has to be higher than 95% with recovery at 90%, to match the transportation/injection requirements.

The MEA absorption process remains the reference today but its energy consumption (about 3 MJ/kg_{CO2}) and the amine consumption are still challenging drawbacks.

The interest of CO_2 capture by indirect TSA (Temperature Swing Adsorption) was demonstrated experimentally in a previous work. The aim of this paper is to present the results of a numerical parametric study. Two main parameters are explored: the desorption temperature (100 to 200 °C) and the purge flow rate (0.1 to 0.5 $Ndm^3.min^{-1}$). Four performance indicators are evaluated: CO_2 purity, recovery, productivity and specific energy consumption.

Results show that purity above 95% can be achieved. Keeping the 95% target, it is possible to achieve recovery at 81% with productivity at 57.7 g_{CO2}/kg_{ads}.h and a specific

energy consumption of 3.23 MJ/kg_{CO2}, which is about the same level than for up to date MEA processes.

Comparison with other adsorption processes exhibits that this process has good potential especially since some improvements are still expected from further research.

Keywords: adsorption, CO_2 capture, numerical study, TSA, zeolite

1. INTRODUCTION

The major issue of post-combustion capture is to produce a highly concentrated CO_2 stream, matching the purity requirement for transportation, although the CO_2 is diluted in the flue gas: between 4% for Natural Gas Combined Cycle (NGCC) and 14% for Pulverised Coal (PC). Furthermore, the process has to be viable from economic and energy aspects so that the energy consumption has to be as low as possible (target around 1 MJ/kg_{CO2} is sometimes quoted) while keeping high CO_2 recovery, above 90%. Chemical absorption (conventional MEA) is today reference process. The heat requested for the amine regeneration, in up to date MEA processes, represents an energy cost ranging from 2.5 to 3.5 MJ/kg_{CO2} (Abu-Zahra et al., 2007, Le Moullec and Kanniche, 2011).

Adsorption could be an alternative to absorption for CO_2 capture. Two main desorption technologies can be used in adsorption processes: TSA (Temperature Swing Adsorption) and PSA/VSA (Pressure/Vacuum Swing Adsorption). Despite their intensive use in other applications (hydrogen purification, VOC recovery, etc.), development is still needed to make them competitive for CO_2 capture (IPCC, 2005).

Intensive experimental and numerical work has been done on PSA/VSA application to CO_2 capture. Some representative results are presented hereafter.

Ishibashi et al. (1996) have proposed one of the first study on using a PTSA cycle for post combustion CO_2 capture. They have managed to reach a purity of 99% with a recovery at 90% using dedicated zeolite. However, the energy penalty was quite important at about 2 $MJ_{el}/kg_{CO2,}$ which is approximately equivalent to 5 $MJ_{heat}/kg_{CO2.}$ Suzuki et al. (1997) have proposed a 2-bed 2-step PSA cycle. They achieved only poor performance in terms of purity (18%) despites a recovery at 90%, as no product recycling was used. Chue et al. (1995) have compared zeolite 13X and activated carbon using a VPSA cycle. They concluded on the superiority of the 13X in this case and achieved high purity (99%) with recovery at 53% and 70% depending on CO_2 molar fraction in the feed. It has to be noticed that these values were quite high compared to the post-combustion ones as 16%-84% CO_2-N_2 and 26%-74% CO_2-N_2 mixtures were used. Na et al. (2001) have also used a VPSA with three beds and seven steps with product recycling. Their recovery was quite low (34%) but the purity was well above the requirement (99,8%). Chou and Chen (2004) have studied VSA process with zeolite 13X and low or high recycling. They have shown that a 2-bed configuration with no recycling cannot match the requirement in purity (between 43 and 48% for a recovery at 88-94%). With a 3-bed configuration and high recycling, they have managed to reach 63% purity but with a recovery decreasing to 70%. The PSA process developed by Park et al. (2002) allows reaching a purity of 70% with a recovery of 30%. To enhance the performances (99% in purity), these authors have proposed a two-stage process. The CO_2CRC team working on the adsorption has made an extensive work on VSA application for CO_2 capture (Zhang et al., 2008, Li et al., 2008). They have used zeolite

13X with a 3-bed VSA. They achieved purity ranging from 90 to 95% with recovery ranging from 60% to 70%. They have also addressed the influence of humidity presence in the feed. Water presence has a dramatic effect on CO_2 adsorption capacity due to strong competition.

Reynolds et al. (2005 and 2006) have evaluated a PSA process working at high temperature with hydrotalcite as adsorbent, which is supposed to be less sensitive to water than zeolite 13X. With four beds, four steps and high product recycling they manage to achieve purity at 82.7% coupled to recovery at 17.4%.

ESA (Electrical Swing Adsorption) has also been explored (Grande and Rodrigues, 2007). The authors used an activated carbon honeycomb monolith. High recovery is achieved (89%) but the purity is only 16%. They suggest to find an alternative adsorbent, as the CO_2 adsorption capacity on activated carbon is low, and to use a product rinse step to increase the purity.

Tlili et al. (2009) have studied the use of an hybrid TSA/VSA (VTSA). The TSA is indirect as the heating is performed through the jacket thanks to a heating wire. They have achieved 99% in purity for both TSA and VSA modes. The recovery depends on the desorption temperature and purge flow rate.

Our Laboratory has been interested in indirect TSA processes since many years. Contrary to PSA/VSA, TSA can be directly heat driven. However, the main drawbacks of TSA are its low productivity, which results in large adsorbent amount and desorbate dilution because of regeneration by hot gas purge. To avoid these drawbacks, an indirect TSA process developed in our laboratory is used (Bonjour et al., 2002, Clausse et al., 2003). The originality of this process comes from the indirect heating during the regeneration step using an internal heat exchanger. Heating is performed in a two-phase

heat transfer mode, namely condensation of steam, while a small purge can be used to help to increase the desorption rate by pushing out the desorbed component and by lowering its partial pressure. This allows reaching high heat transfer coefficients, which reduces the regeneration time. During the adsorption step, the adsorber is cooled by water circulation that allows removing the adsorption heat and limits the impact of the inlet gas temperature. Then, the adsorbent capacity is kept maximal.

Previous experimental works has allowed us to highlight the benefit of using zeolite 5A vs. 13X (Mérel et al., 2006 and 2008) and the interest of this process for CO_2 capture. The aim of the present work is to use a numerical model to explore the sensitivity of this process to variations in desorption temperature and purge flow rate. After the presentation of the model equations and validation, results for desorption temperature range of 100 to 200°C and purge flow rate from 0.1 $Ndm^3.min^{-1}$ to 0.5 $Ndm^3.min^{-1}$ are presented.

2. MODEL

2.1 Operating conditions

The exhaust gases are simulated by a dry N_2/CO_2 mixture as it was the case in our previous experimental work (Mérel et al., 2003).

The adsorbent is 5A zeolite supplied by AXENS (IFP Group Technologies). The small spherical beads have an average diameter of 2 mm while the density is about 730 kg/m^3. For the equilibrium isotherms, the data given by Wang and LeVan (2009) were used for CO_2 and for N_2 those of Vereist and Baron (1985). They are reported on figure 1 and 2, respectively. From this pure component data, it appears that the affinity of the 5A is far

stronger with CO_2 than with N_2. Indeed, assuming that no competitive adsorption occurs between N_2 and CO_2, the adsorbed amounts are 0.25 $mol.kg^{-1}$ and 3 $mol.kg^{-1}$ at 25 °C and atmospheric pressure for a 90% N_2 – 10% CO_2 mixture (molar basis). Because of competitive adsorption, the amount of nitrogen will be even smaller during adsorption step. This was confirm from the breakthrough experiments done in our previous work where we found that the CO_2 adsorbed amount was close to that given by the pure component equilibrium data (Mérel et al., 2006 and 2008). Hence, the co-adsorption of nitrogen is neglected in this work as this assumption has already proven to give consistent results (Mérel, 2009).

To describe the isotherms of the CO_2, the Toth equation, which was chosen by Wang and LeVan (2009), is used:

$$n = \frac{aP}{\left[1 + (bP)^t\right]^{1/t}} \tag{1}$$

where n is the adsorbed amount ($mol.kg^{-1}$), P the component partial pressure (kPa) and a b, and t Toth equations parameters. Their temperature dependence is given by:

$$b = b_0 \exp\left(\frac{E}{T}\right) \tag{2}$$

$$a = a_0 \exp\left(\frac{E}{T}\right) \tag{3}$$

$$t = t_0 + \frac{c}{T} \tag{4}$$

Parameter values are listed in table 1.

It has to be noticed that zeolite 5A has a strong affinity with water, which implies a degradation of the CO_2 loading because of competitive adsorption (Li et al., 2008, Wang and LeVan, 2010). However this major issue for post-combustion capture will not be addressed as part of this work as the main goal is to evaluate the potential of indirect TSA for this application: it is presumed that a pre-treatment (water removal by condensation or adsorption on silica-gel for example) is used.

The adsorber is made of two concentric tubes with twelve fins welded on the inner one. The adsorbent fill the annulus space. As the fins are equally distributed, large and small channel exist corresponding to angles of 50° and 10° between the fins. For a more detailed presentation, reader should report to previous work: Bonjour et al. (2002), Clausse et al., (2003 and 2004).

We use a 2-step cycle: adsorption and desorption, without any pre-heating or pre-cooling step in-between (Figure 3). During adsorption, cooling water flows in the inner tube allowing removing the heat of adsorption from the adsorbent bed so that the performances are close to that achieved during isothermal adsorption. The N_2/CO_2 mixture enters the bed (annulus section) and the CO_2 is adsorbed by the zeolite. As the goal is to capture CO_2 and not to purify nitrogen, CO_2 breakthrough can be allowed at the outlet if needed. When the adsorption step is stopped, desorption starts immediately by admitting saturated steam in the inner tube. A small purge is used in order to help the desorbed CO_2 to flow out of the bed. The operating conditions used for this work are resumed hereafter:

For adsorption, the feed has a total flow rate of 20 $Ndm^3.min^{-1}$, an inlet temperature of 20 °C and the gas composition is 90%$_{vol.}$ N_2 and 10%$_{vol.}$ CO_2. During this step, the cooling water temperature is set at 16 °C. The adsorption step stops when the outlet CO_2

concentration reaches 50% of that at the inlet with positive gradient evolution. The gradient checking is necessary as the 50% concentration value is also reached at the beginning of the adsorption step when the bed is cooled down while the CO_2 concentration decreases from above 90% (end of desorption step) to value below the feed concentration.

During the desorption step, the N2 purge has a flow rate between 0.1 and 0.5 $Ndm^3.min^{-1}$ and a temperature between 100 and 200 °C. The desorption ends when the CO_2 outlet fraction reaches 90% with negative gradient evolution. As for the adsorption step, the gradient checking is mandatory since at the beginning of the desorption step the concentration increases from nearly 50% (end of adsorption) to above 90% but resulting in a positive gradient evolution. The next adsorption step starts immediately after.

2.2 Equations

The model is based on previous work in our Laboratory (Clausse et al., 2004). The following assumptions are made:

- the gases behave as ideal gases
- the gradients of temperature, concentration and velocity in the radial and angular direction are neglected (1D model)
- the Linear Driving Force Model (LDF) applies for representing the mass transfer inside the adsorbent

- The local thermal equilibrium (LTE) between the gas and solid phases is assumed. This assumption has already been validated for our process (Clausse et al., 2004, Bonjour et al., 2002)

The component mass balance is written as:

$$\frac{\partial C_i}{\partial t} = -\frac{\partial u C_i}{\partial z} + D_{ax}\frac{\partial^2 C_i}{\partial z^2} - \frac{1-\varepsilon}{\varepsilon}\rho_{ads}\frac{\partial n_i}{\partial t} \quad (1)$$

where C_i is the component concentration in the gas phase ($mol.m^{-3}$), u the interstitial velocity ($m.s^{-1}$), D_{ax} the axial dispersion coefficient ($m^2.s^{-1}$), ε the bed porosity, ρ_{ads} the particle density ($kg_{ads}.m^{-3}$) and n_i the i^{th} component concentration in the adsorbed phase ($mol.kg_{ads}^{-1}$). The same equation, without the source term $\frac{\partial n_i}{\partial t}$, is used for nitrogen. The momentum equation represented by Darcy's equation is written as:

$$-\frac{\partial P}{\partial z} = \frac{150\mu(1-\varepsilon)^2}{\varepsilon^2 d_p^2} \quad (2)$$

with P the pressure (Pa), μ the dynamic viscosity (Pa.s), d_p the adsorbent bead mean diameter (m).

Taking into account the assumptions, the energy balance equation is written as:

$$\frac{\partial T}{\partial t} = \frac{\eta_{fin} h \Sigma \left(T_{wall} - T\right) - \varepsilon \sum_i \bar{c}_{p,i} \frac{\partial u C_i T}{\partial z}}{(1-\varepsilon)\rho_{ads}(c_{p,ads} + c_{p,liq,CO2} \cdot n_{CO2} \cdot \overline{M}_{CO2})} + \frac{\sum_i \Delta \overline{H}_i \frac{\partial n_i}{\partial t}}{\rho_{ads}(c_{p,ads} + c_{p,liq,CO2} \cdot n_{CO2} \cdot \overline{M}_{CO2})} \quad (3)$$

with T the temperature (K), $c_{p,ads}$ the adsorbent heat capacity ($J.kg^{-1}.K^{-1}$), $\bar{c}_{p,i}$ the i^{th} component molar heat capacity ($J.mol^{-1}.K^{-1}$), η_{fin} the fins efficiency, h the convective heat transfer coefficient between the gas and the wall ($W.m^{-2}.K^{-1}$), Σ the heat transfer area per unit column volume ($m^2.m^{-3}$), T_{wall} the wall temperature (K) and ΔHi the i^{th} component isosteric heat of adsorption ($J.mol^{-1}$). The value of the ηh product has been obtained thanks to a numerical model validated with various experiments (Bonjour, Chalfen and Meunier, 2002). For the adsorbed phase thermal inertia, only the CO_2 adsorbed amount is taken into account as the nitrogen adsorption is neglected. The thermal capacity is supposed equal to that of the liquid. Parameters are listed in table 2.
The set of PDE/DAE is solved using the method of lines and DASPK 2.0 mathematical solver.

2.2 Model Validation

Figure 4 represents the numerical and experimental breakthrough curves for a total flow rate of 20 $Ndm^3.min^{-1}$, a CO_2 inlet molar fraction of 10%, an inlet temperature of 20 °C and a cooling water temperature of 16 °C (tap water), while the temperature evolutions are reported on figure 5. A reasonable agreement between numerical and experimental

curves is obtained. The deviations are due to the 1D geometry and adiabatic conditions chosen for the model, while 3D effects (fin distribution) and heat losses to the surroundings exist (Bonjour et al., 2002, Clausse et al., 2004).

The CO_2 outlet molar fraction and the temperature evolutions are reported on figure 6 for the desorption of a bed initially saturated at 10% CO_2 and at a temperature of 16 °C. The desorption temperature is 150 °C while the purge flow rate is 0.2 $Ndm^3.min^{-1}$. The model fits very well for the concentration and reasonably well for the temperature. Again, the deviations for the temperature are due the 3D behaviour of the adsorber. This aspect is highlighted by the reported evolution of two different temperatures: small channel with an angle of 10° between fins and large channel with an angle of 50°. Moreover, the heat losses to the ambient are neglected in the model. This temperature distribution results in a distribution of the adsorbed quantities, which impacts the desorption rate as illustrated on figure 7. The curve shape of the predicted flow rate is similar to that obtained form experimental results. However, the model slightly overestimates the value, as the temperature is homogeneous contrarily to the experiment. It has to be reminded adsorbers at industrial size have a near adiabatic behaviour, which tends to make the temperature homogeneous.

The parameters were also tested for cyclic operation and the numerical results match the experimental ones reasonably well (figure 8). The continuous breakthrough during adsorption (between 260 and 320 min for example) can be seen as well. The minimum CO_2 molar faction is 0.4 % and desorption starts when the CO_2 concentration starts to increase. The difference for the thermal wave amplitudes comes again from the 3D thermal effects taking place in the prototype adsorber.

As a consequence, the parameters are kept constant for the parametric study presented in this article, as they were identified as reliable to predict a wide range of results (Mérel, 2009).

3. PARAMETRIC STUDY

Cyclic operations were run for different operating conditions. The desorption temperature ranged between 100 to 200 °C while the purge flow rate ranges from 0.1 $Ndm^3.min^{-1}$ to 0.5 $Ndm^3.min^{-1}$. The feed flow rate during adsorption is always equal to 20 $Ndm^3.min^{-1}$ with 10% of CO_2 (molar basis). The feed temperature is equal to 20 °C and the cooling water temperature 20 °C.

The adsorption stops when the outlet CO_2 molar fraction is equal to 5 % (50% of the feed value) with positive derivative. The desorption ends when the CO_2 molar fraction is equal to 90 % with negative derivative, in order to achieve at least a purity equal to this value. About 4 to 6 cycles are needed to reach the cycle steady state (CSS) at which the performances are evaluated. Four indicators are considered:

- CO_2 purity, which is the CO_2 average molar fraction during the desorption step
- CO_2 recovery, which represents the fraction of CO_2 recovered during the desorption step compared to the total amount in the feed
- CO_2 productivity is defined as the mass of CO_2 recovered during desorption divided by the total adsorbent mass and overall cycle time
- CO_2 specific consumption is defined as total energy used for heating divided by the recovered mass of CO_2

3.1 Results

Figure 9 shows the CO_2 purity versus desorption temperature for various purge flow rates. We can notice that the purity increases with the desorption temperature at given purge while the CO_2 is more diluted when increasing the purge at constant desorption temperature. Taking into account the 95% target for CO_2 purity, a minimum desorption temperature of 115 °C is requested for a 0.1 $Ndm^3.min^{-1}$ purge. This temperature increases to 200 °C for a purge at 0.5 $Ndm^3.min^{-1}$.

Figure 10 presents the productivity versus desorption temperature for various purge flow rates. A high purge flow rate results in an increase in productivity. Indeed, keeping the operating conditions allowing to achieve a 95% purity we can found a productivity of 40 $g_{CO2}.kg_{ads}^{-1}.h^{-1}$ at 0.1 $Ndm^3.min^{-1}$/115 °C compared to 65.1 at 0.5 $Ndm^3.min^{-1}$/200 °C. At temperature above 150 °C, we can notice that for purge flow rate higher than 0.2 $Ndm^3.min^{-1}$, the productivity is nearly independent of purge flow rate. Hence, at high desorption temperature, there is no interest to increase the flow rate in terms of productivity which allow to reach high CO_2 purity: 95.5 % at 0.2 $Ndm^3.min^{-1}$ compared to 92.5 % at 0.5 $Ndm^3.min^{-1}$, for a desorption temperature of 150 °C in both cases. At lower temperatures, the purge influence on productivity is noticeable. This phenomenon is directly linked to the criterion chosen to ends the desorption step. Indeed, for a given desorption temperature, the CO_2 is more diluted at high purge than low purge so that the 90 % criterion is reached faster. Hence at T_{des} = 100 °C, the desorption lasts 31 min (112 g of CO_2 desorbed) for 0.1 $Ndm^3.min^{-1}$, while it lasts only 6.8 min (25 g of CO_2 desorbed) at 0.5 $Ndm^3.min^{-1}$. On the other hand, the overall cycle lasts 82 and 38 min respectively. As the CO_2 desorbed mass decreases faster than the

overall cycle time, the productivity drops when increasing the purge. In comparison, at T_{des} = 150 °C, for the same purge values, the overall cycle durations are 113 min and 84 min, respectively. It corresponds to CO_2 desorbed mass of 258 and 205 g so that the ratio between the two cycle durations and between the desorbed masses are of the order of magnitude resulting in similar values for productivity.

The CO_2 recovery ratios are reported on figure 11. The 90% target is not achieved for the studied operating conditions with a maximum at 88% for T_{des} = 200°C and 0.1 $Ndm^3.min^{-1}$ purge. As it can be seen, the recovery increases with the temperature while it decreases when the purge increases. The non-recovered CO_2 is due to the breakthrough at the end of the adsorption step (adsorption ends when the outlet CO_2 molar fraction is equal to 50% of the feed) but also to the continuous breakthrough during the adsorption step, as the CO_2 outlet molar fraction never falls to zero: on figure 8 the minimum CO_2 concentration is equal to 0.4%. At high purge, the desorption step end occurs rapidly because of dilution so that the adsorber is less regenerated than at low purge. As consequence, the adsorption capacity is smaller for the next adsorption step resulting in an important breakthrough. The same reasoning can be applied for the desorption temperature influence. At given purge flow rate, the desorbed amount increases as the desorption temperature increases, resulting in a better-regenerated bed. Furthermore, the cooling is efficient during the beginning of the adsorption step (Bonjour et al. 2003, Clausse et al., 2004) so that the adsorption capacity increases faster for a bed regenerated at high temperature.

The specific energy consumption evolutions are reported on figure 12. The minimum is around 3.22 $MJ.kg_{CO2}^{-1}$, which is about the same level than the heat consumption for the up to date amine MEA process (2.5-3.5 MJ/kg_{CO2}). At low desorption temperatures,

below 140 °C, the specific consumption increases rapidly when the temperature decreases and the influence of the purge is noticeable too: the lowest the purge flow rate, the lowest the energy consumption. For higher temperatures, above 150 °C, the specific consumption is almost constant (between 3.22 and 3.36 $MJ.kg_{CO2}^{-1}$) with a slight increase at high temperatures. The behaviour is due to the trade-off between the CO_2 desorbed mass and the energy consumption. At low desorption temperature, the temperature swing is limited resulting in low energy consumption but also low desorbed mass. The effect is amplified with high purge which results in a dilution of the effluent meaning shorter desorption step and even lower desorbed mass. For example, at T_{des} = 100 °C and a 0.5 $Ndm^3.min^{-1}$ purge, we obtain a specific consumption of 7.72 MJ/kg_{CO2}^{-1} corresponding to 24.77 g of CO_2 cycled and an energy consumption of 191 kJ. At the same desorption temperature but with a 0.1 $Ndm^3.min^{-1}$ purge we get a specific consumption of 3.75 $MJ.kg_{CO2}^{-1}$ corresponding to 112 g of cycled CO_2 and an energy consumption of 420 kJ.

From these different results, we have retained the following operating conditions and performances. Fixing the purity at 95% and choosing the minimum energy consumption, we get the following operating parameters: T_{des} = 160 °C and a purge at 0.3 $Ndm^3.min^{-1}$. The performances are: CO_2 purity 95%, CO_2 recovery 81%, CO_2 productivity 57.7 $g.kg_{ads}^{-1}.h^{-1}$ and a specific consumption of 3.23 $MJ.kg_{CO2}^{-1}$. It has to be noticed that the productivity is also equal to 41.5 $kg_{CO2}.m_{ads}^{-3}.h^{-1}$, which is of the same order of magnitude than, the productivity deduced form the work of Tobiesen and Svendsen (2006) for a MEA process (39 $kg_{CO2}.m_{ads}^{-3}.h^{-1}$). This tends to prove that adsorption process can have a footprint comparable of that of MEA process for CO_2 capture.

3.2 Comparison with other CO_2 capture processes

The performances found in the literature of PSA, VSA and ESA processes for CO_2 capture are reported in Table 3. The values for MEA and those for our TSA found in section 3.1 are reported as well.

This process is able to achieve high values for both the purity and recovery contrary to the majority of the others adsorption processes. Furthermore, these performances are achieved with a feed at only 10% of CO_2 compared to value between 12 and 20% for the other studies.

In terms of energy savings, the specific energy consumption is close to that requested for heating in MEA absorption process (3 $MJ.kg_{CO2}^{-1}$). Compared to PSA/VSA results, the energy consumption is higher. However, it has to be reminded that the values for VSA/PSA processes are given in terms of electricity while it is heat for TSA or absorption. Hence, the comparison could not be directly made as the primary energy to electricity conversion ratio is needed.

4 CONCLUSION

The aim of this work was to present a numerical study on CO_2 capture by indirect TSA. After model validation, comparing with previous experimental results, a parametric study was performed with desorption temperature ranging from 100 °C to 200 °C and purge flow rate from 0.2 to 0.5 $Ndm^3.min^{-1}$.

An increase in desorption temperature results in an increase in CO_2 purity, recovery and productivity. The specific consumption present a minimum occurring at different

desorption temperature depending on the purge flow rate. It has to be noticed that the productivity is higher at low purge for desorption temperature below 130 °C while at higher desorption temperature a high flow rate increases the productivity. However, the difference between 0.2 $Ndm^3.min^{-1}$ and 0.5 $Ndm^3.min^{-1}$ remains scarce (63.5 and 65 $g.kg_{ads}^{-1}.h^{-1}$ at T_{des} = 200 °C, respectively).

As reference performances, we have fixed the purity at 95% (requirement for transportation and injection). Choosing the minimum energy consumption for this purity, we get the following operating parameters: T_{des} = 160 °C and a purge at 0.3 $Ndm^3.min^{-1}$. The performances are: CO_2 purity 95%, CO_2 recovery 81%, CO_2 productivity 57.7 $g.kg_{ads}^{-1}.h^{-1}$ and a specific consumption of 3.23 $MJ.kg_{CO2}^{-1}$. Moreover, the productivity is similar to results found for MEA process. These performances compares well with the results obtained for VSA/PSA processes and are encouraging, despite a full work on process integration has to be done to estimate the real energy penalty.

To enhance the process performances, different ways would have to be considered. A first step would be to use a pre-cooling step in order to increase the recovery by limiting the CO_2 breakthrough occurring at the beginning of the adsorption step when the bed is at high temperature. To increase the productivity while lowering the energy consumption, the use of a hybrid VTSA process could be of interest. This might allow to decrease the desorption temperature but a trade-off between heat and electrical consumption has to be found. Furthermore, the influence of the cooling temperature and of feed composition and temperature has to be addressed as well.

REFERENCES

Abu-Zahra, M. R. M., Schneiders, L. H. J., Niederer, J. P. M., Feron, P. H. M., Versteeg, G.F., 2007. CO_2 capture from power plants Part I. A parametric study of the technical performance based on monoethanolamine. Int. J. Greenhouse Gas Control 1, 37-46.

Bonjour, J., Chalfen, J.B., & Meunier, F., 2002. Temperature swing adsorption process with indirect cooling and heating. Ind. Eng. Chem. Res. 41(23), 5802-5811.

Choi, W.K., Kwon, T.I., Yeo, Y.K., Lee, H., Song, H.K., Na, B.K., 2003. Optimal operation of the pressure swing adsorption (PSA) process for CO_2 recovery. Korean J. Chem. Eng. 20(4), 617-623

Chou, C. Chen, C., 2004. Carbon dioxide recovery by vacuum swing adsorption. Sep. Purif. Technol. 39, 51-65

Chue, K.T., Kim, J.N., Yoo, Y.J., Cho, S.H., Yang, R.T., 1995. Comparison of activated carbon and zeolite 13X for CO2 recovery from flue gas by pressure swing adsorption. Ind. Eng. Chem. Res. 34, 591-598

Clausse, M., Bonjour, J., Meunier, F., 2003. Influence of the presence of CO2 in the feed of an indirect heating TSA process for VOC removal. Adsorption 9, 77-85

Clausse, M., Bonjour, J., Meunier, F., 2004. Adsorption of gas mixtures in TSA adsorbers under various heat removal conditions. Chem. Eng. Sci. 59(17), 3657-3670

Grande, C., Rodrigues, A., 2008. Electrical Swing adsorption for CO_2 removal from flue gases. Int. J. Greenhouse Gas Control 2, 194-202

IPCC, (2005). IPCC Special Report on Carbon Dioxide Capture and Storage. Prepared by Working Group III of the Intergovernmental Panel on Climate Change [Metz, B., O. Davidson, H. C. de Coninck, M. Loos, and L.A. Meyer (eds.)]. Cambridge University Press, Cambridge, United Kingdom and New York, NY, USA, 442 p.

Ishibashi, M., Ota, H., Akutsu, N., Umeda, S., Tajika, M., Izumi, J., Yasutake, A., Kabata, T., Kageyama, Y., 1996. Technology for removing carbon dioxide from power plant flue gas by the physical adsorption method. Energy Convers. Mgmt. 37, 929-993

Ko, D., Siriwardane, R., Biegler, L.T., 2005. Optimization of pressure swing adsorption and fractionated vacuum pressure swing adsorption processes for CO2 capture. Ind. Eng. Chem. Res. 44, 8084-8094

Le Moullec, Y., Kanniche, M., 2011. Screening of flowsheet modifications for an efficient monoethanolamine (MEA) based post-combustion CO_2 capture. Int. J. Greenhouse Gas Control, doi:10.1016/j.ijggc.2011.03.004

Li, G., Xiao, P., Webley, P., Zhang, J., Singh, R. and Marshall, M., 2008. Capture of CO2 from high humidity flue gas by vacuum swing adsorption with zeolite 13X. Adsorption 14, 415-422

Mérel, J., Clausse, M., Meunier, F., 2006. Carbon dioxide capture by indirect thermal swing adsorption using 13X zeolite. Env. Prog. 25(4). 327-333

Mérel, J., Clausse, M., Meunier, F., 2008. Experimental investigation on CO_2 post-combustion capture by indirect thermal swing adsorption using 13X and 5A zeolites. Ind. Eng. Chem. Res. 47, 209-215

Mérel, J., 2009. Etude du captage post-combustion du CO_2 grâce à un procédé TSA (Temperature Swing Adsorption) à chauffage et refroidissement indirects. Ph-D thesis, Conservatoire National des Arts et Métiers. 182 p.

Na, B.K., Koo, K.K., Eum, H.M., Lee, H., Song, H.K., 2001. CO_2 recovery from flue gas by PSA process using activated carbon. Korean J. Chem. Eng. 18, 220-227

Park, J., Beum, H., Kim, J., Cho, S., 2002. Numerical analysis on the power consumption of the PSA process for recovering CO_2 from flue gas. Ind. Eng. Chem. Res. 41, 4122-4131

Reynolds, S.P., Ebner, A.D., Ritter, J.A., 2005. New pressure swing adsorption cycles for carbon dioxide sequestration. Adsorption 11, 531-536

Reynolds, S.P., Ebner, A.D., Ritter, J.A., 2006. Stripping PSA cycles for CO_2 recovery from flue gas at high temperature using a hydrotalcite-like adsorbent. Ind. Eng. Chem. Res. 45, 4278-4294

Suzuki, T., Sakoda, A., Suzuki, M., Izumi, J., 1997. Recovery of carbon dioxide from stack gas by piston-driven ultra-rapid PSA. J. Chem. Eng. Jpn. 30, 1026-1033

Tlili, N., Grévillot, G., Vallières, C., 2009. Carbon dioxide capture and recovery by means fo TSA and/or VSA. Int. J. Greenhouse Gas Control 3, 519-527

Tobiesen, A., Svendsen, H.F., 2006. A comparative study of experimental and modelling performance results from CASTOR Esbjerg Pilot Plant. 8th International Conference on Greenhouse Gas Control Technologies (GHGT-8), Trondheim, Norway, November 19-22

Vereist, H., Baron, G. V., 1985. Adsorption of Oxygen, Nitrogen, and Argon on 5A Molecular Sieve. J. Chem. Eng. Data. 30, 66

Wang, Y., LeVan, M.D., 2009. Adsorption equilibrium of carbon dioxide and water vapor on zeolites 5A and 13X and Silica Gel: Pure Components. J. Chem. Eng. Data. 54, 2839-2844

Wang, Y., LeVan, M.D., 2010. Adsorption equilibrium of binary mixture of carbon dioxide and water vapor on zeolites 5A and 13X. J. Chem. Eng. Data. 55, 3189-3195

Zhang, J., Webley, P.A., Xiao, P., 2008. Effect of process parameters on power requirements of vacuum swing adsorption technology for CO_2 capture from flue gas. Energy Convers. Mgmt. 49, 346-356

Table 1. Toth equation parameters for CO_2/5A (Wang and LeVan, 2009)

a_0 mol.kg^{-1}.kPa^{-1}	b_0 kPa^{-1}	E K	t_0 (-)	c K
9.875×10^{-7}	6.761×10^{-8}	5.625×10^{-3}	2.700×10^{-1}	-2.002×10^{-1}

Table 2. Parameter values

Parameter	Unit	Values
adsorber length	m	1
adsorber outer diameter	m	0.072
adsorber inner diameter	m	9.5×10^{-3}
ρ_{ads}	$kg.m^{-3}$	1161
$c_{p,ads}$	$J.kg^{-1}K^{-1}$	920
ε	-	0.38
particle diameter	mm	2
Σ	$m^2.m^{-3}$	177.8
ΔH_{CO2}	$J.mol^{-1}$	45000
k	s^{-1}	0.1
D_{ax}	$m^2.s^{-1}$	10^{-5}
h_{ads}	$W.m^{-2}.K^{-1}$	20
h_{des}	$W.m^{-2}.K^{-1}$	20

Table 3. Comparison of several CO_2 capture processes

Ref	CO_2 feed molar fraction (%), (other gas present)	CO_2 purity (%)	CO_2 recovery (%)	Specific consumption (Amine/TSA: $MJ_{heat.}/kg_{CO2,\ captured}$) ($PSA : MJ_{el.}/kg_{CO2,\ captured}$)
Amine				
IPCC (2005) and Aroonwilas et al.(2006)	-	99	98	4.2 - 4.8
ESA				
Grande and Rodrigues (2008)	10	23.33	92.57	
PSA/VSA				
Chue et al. (1995)	16 (O_2)	99	53 - 70	-
Ishibashi et al. (1996)	10	99	-	2
Suzuki et al. (1997)		18	90	-
Na et al. (2001)	17	99.5 - 99.8	34 - 69	-
Park et al. (2002)	10	50 - 70	30 - 90	0.09 - 1.1
Choi et al. (2003)	13 (O_2)	99.5	69	-
Chou et Chen (2004)	20	58 - 63	70 - 75	-
Ko et al. (2005)	15	90	90	0.14
Reynolds et al. (2005)	15 (H_2O)	59	87	-
Reynolds et al. (2006)	15 (H_2O)	82.7	17.4	-
Zhang et al. (2008)	12	90 – 95	60 – 70	9.10^{-4} - 15.10^{-4}
TSA				
this work	10	95	81	3.23

Figures Captions

Figure 1. Adsorption isotherms of CO_2 on zeolite 5A (Wang and LeVan. 2009)

Figure 2. Adsorption isotherms of N_2 on zeolite 5A (Vereist and Baron. 1985)

Figure 3. Two-step indirect TSA cycle

Figure 4. Comparison of numerical (line) and experimental (△) breakthrough curves (20 NL/min. y_{co2} = 0.1. T_{inlet} = 20 °C. T_{water} = 16 °C)

Figure 5. Comparison of numerical (thin) and experimental (bold) temperature evolutions during breakthrough at different bed locations: inlet, middle and outlet (20 $Ndm^3.min^{-1}$. y_{co2} = 0.1. T_{inlet} = 20 °C. T_{water} = 16 °C)

Figure 6. CO_2 outlet molar fraction and temperature evolution during desorption at T_{des} = 150 °C and purge flow rate of 0.2 $Ndm^3.min^{-1}$. Comparison of experimental and numerical results.

Figure 7. CO_2 mass flow rate evolution during desorption at T_{des} = 150 °C with a purge flow rate of 0.2 $Ndm^3.min^{-1}$. Comparison of experimental (◇) and numerical (line) results.

Figure 8. Comparison of numerical and experimental results during adsorption/desorption cycles (feed: 20 $Ndm^3.min^{-1}$. y_{co2} = 0.1. T_{inlet} = 20 °C. T_{water} = 16 °C desorption: T_{des} = 150 °C and purge = 0.2 $Ndm^3.min^{-1}$)

Figure 9. CO_2 purity for various desorption temperature and purge flow rate (□ 0.1 $Ndm^3.min^{-1}$. △ 0.2 $Ndm^3.min^{-1}$. ○ 0.3 $Ndm^3.min^{-1}$. ◇ 0.4 $Ndm^3.min^{-1}$. × 0.5 $Ndm^3.min^{-1}$)

Figure 10. CO_2 productivity for various desorption temperature and purge flow rate (□ 0.1 $Ndm^3.min^{-1}$. △ 0.2 $Ndm^3.min^{-1}$. ○ 0.3 $Ndm^3.min^{-1}$. ◇ 0.4 $Ndm^3.min^{-1}$. × 0.5 $Ndm^3.min^{-1}$)

Figure 11. CO_2 recovery for various desorption temperature and purge flow rate (□ 0.1 $Ndm^3.min^{-1}$. △ 0.2 $Ndm^3.min^{-1}$. ○ 0.3 $Ndm^3.min^{-1}$. ◇ 0.4 $Ndm^3.min^{-1}$. × 0.5 $Ndm^3.min^{-1}$)

Figure 12. CO_2 specific consumption for various desorption temperature and purge flow rate (□ 0.1 $Ndm^3.min^{-1}$. △ 0.2 $Ndm^3.min^{-1}$. ○ 0.3 $Ndm^3.min^{-1}$. ◇ 0.4 $Ndm^3.min^{-1}$. × 0.5 $Ndm^3.min^{-1}$)

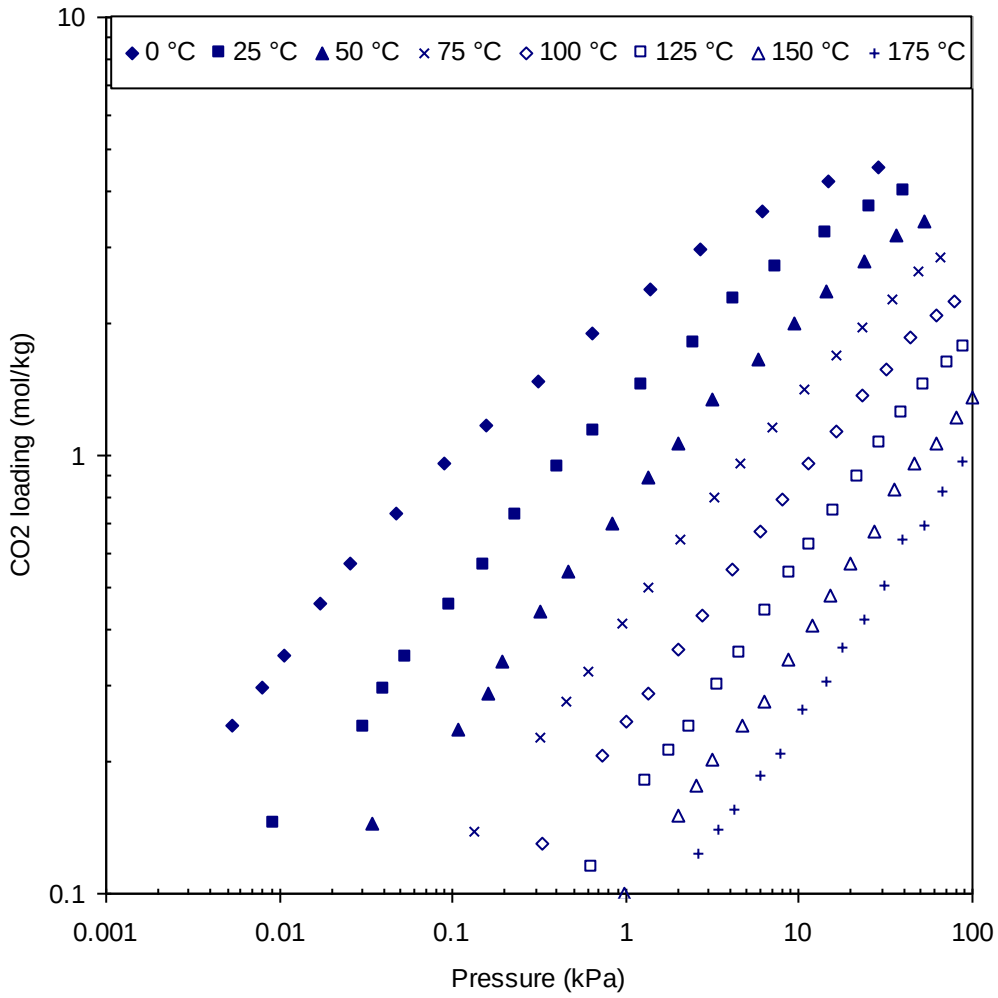
0 °C
25 °C
50 °C
75 °C
100 °C
125 °C
150 °C
175 °C
CO2 loading (mol/kg)
10
1
0.1
0.001
0.01
0.1
1
10
100
Pressure (kPa)

Figure 1

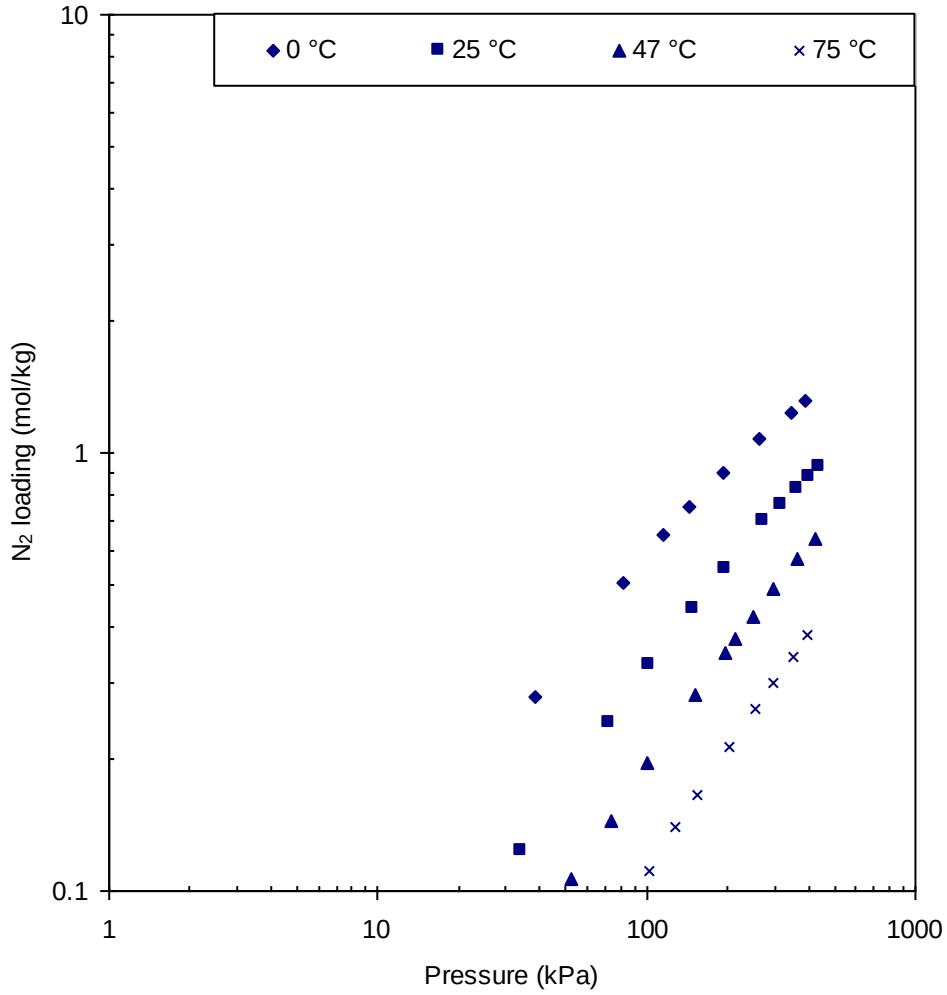
10
1
0.1
N2 loading (mol/kg)
0 °C
25 °C
47 °C
75 °C
1
10
100
1000
Pressure (kPa)

Figure 2

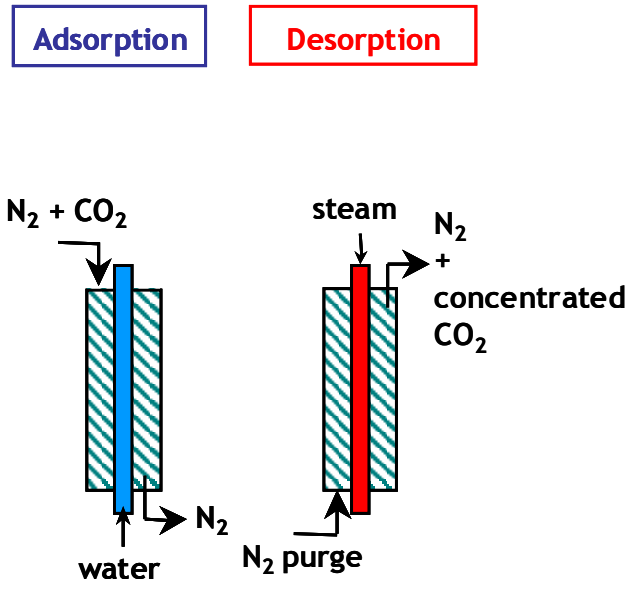
Adsorption
Desorption
$N_2 + CO_2$
steam
N_2
+
concentrated
CO_2
N_2
water
N_2 purge

Figure 3

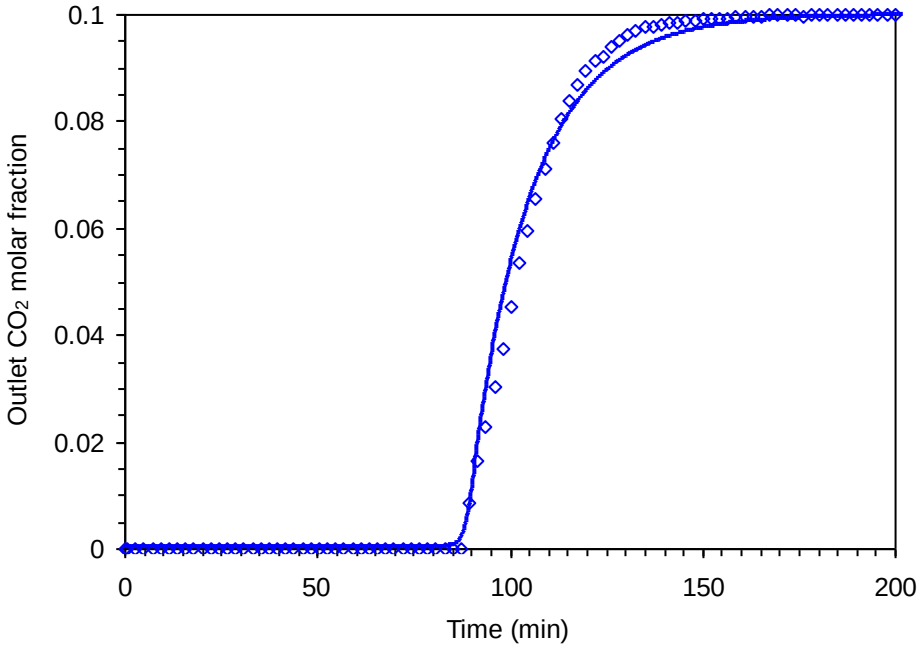
0.1
0.08
0.06
0.04
0.02
0
Outlet CO2 molar fraction
0
50
100
150
200
Time (min)

Figure 4

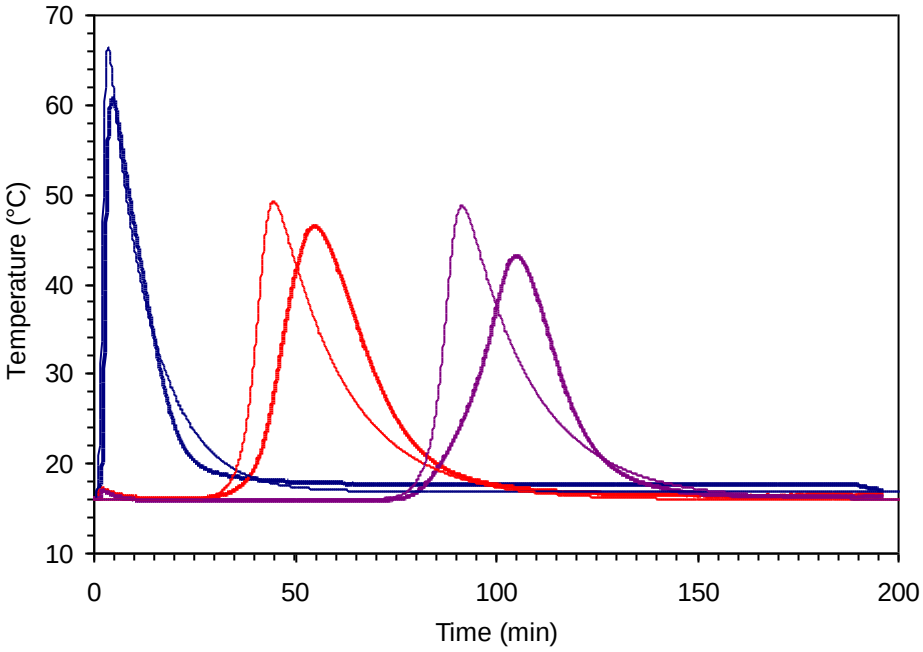

Figure 5

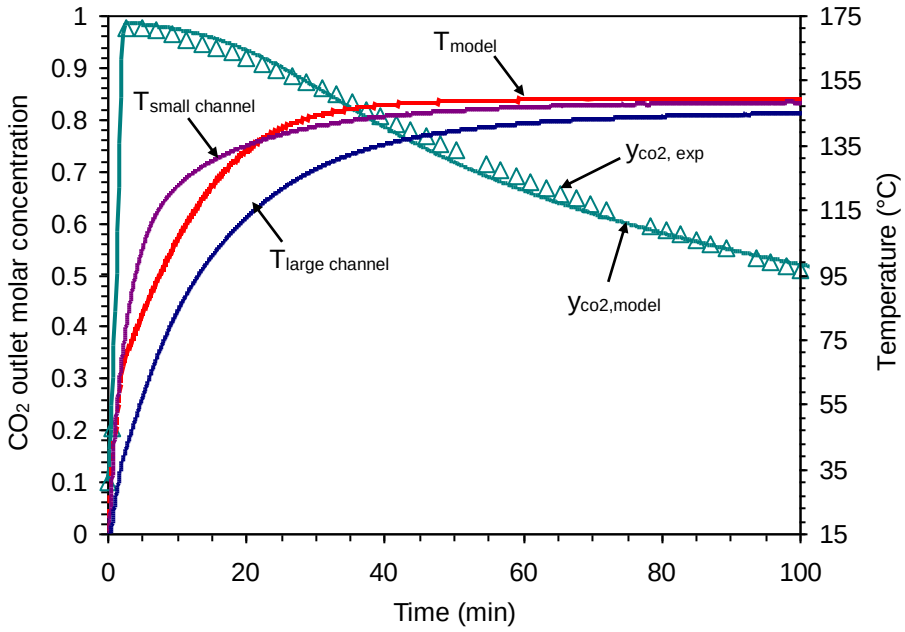
T model
T small channel
T large channel
yco2, exp
yco2,model
CO2 outlet molar concentration
Temperature (°C)
Time (min)
0
0.1
0.2
0.3
0.4
0.5
0.6
0.7
0.8
0.9
1
15
35
55
75
95
115
135
155
175
0
20
40
60
80
100

Figure 6

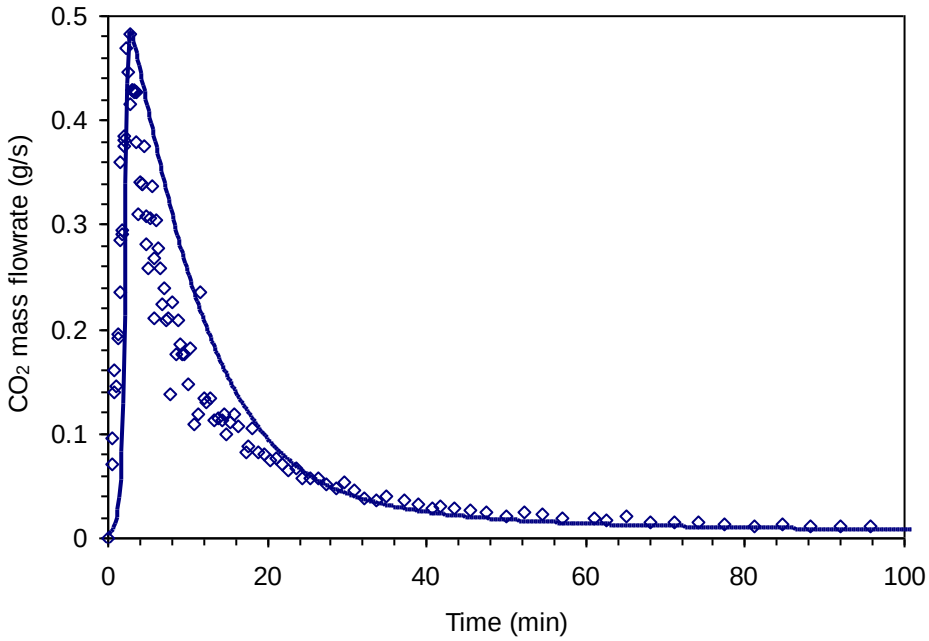

Figure 7

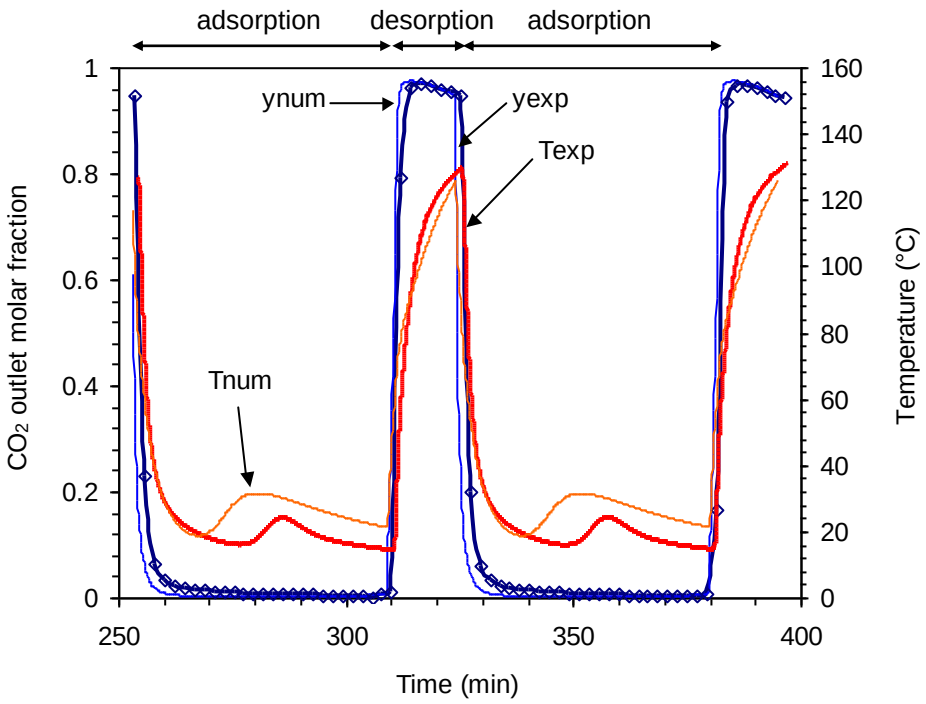
adsorption
desorption
adsorption
ynum
yexp
Texp
Tnum
CO2 outlet molar fraction
Temperature (°C)
Time (min)
0
0.2
0.4
0.6
0.8
1
0
20
40
60
80
100
120
140
160
250
300
350
400

Figure 8

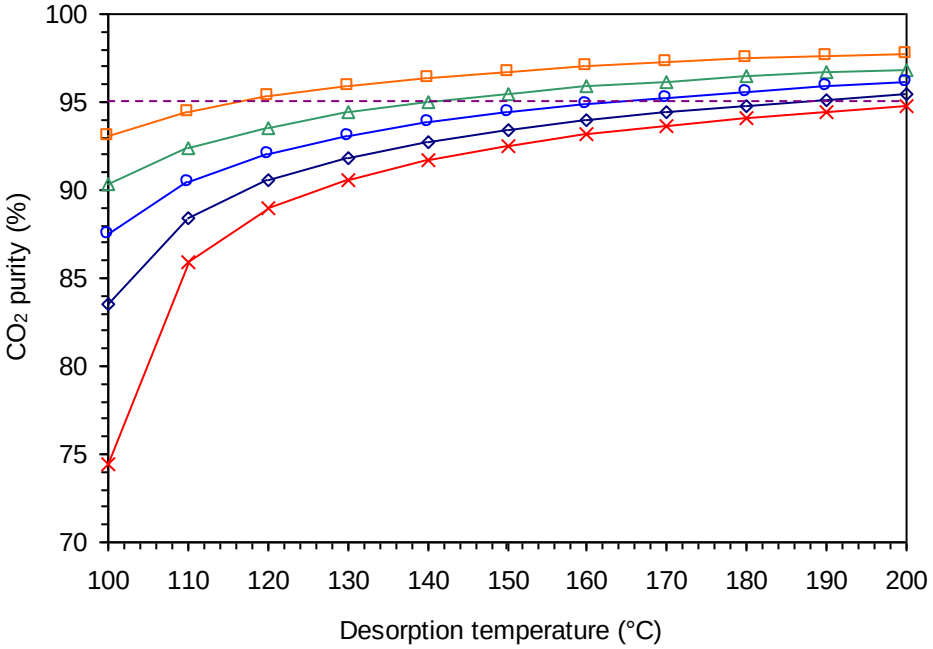
100
95
90
85
80
75
70
CO2 purity (%)
100
110
120
130
140
150
160
170
180
190
200
Desorption temperature (°C)

Figure 9

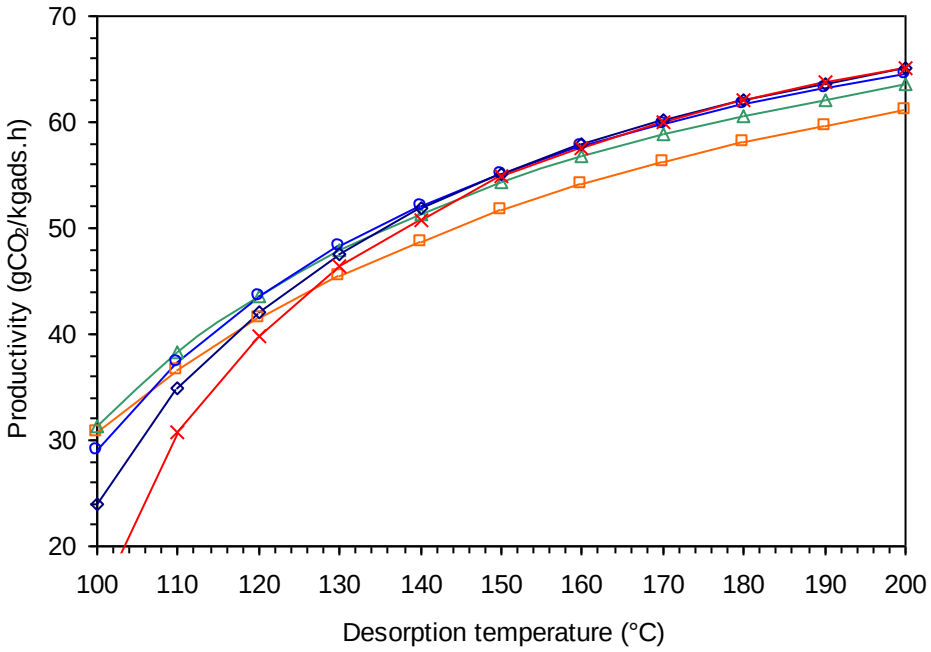
70
60
50
40
30
20
Productivity (gCO2/kgads.h)
100
110
120
130
140
150
160
170
180
190
200
Desorption temperature (°C)

Figure 10

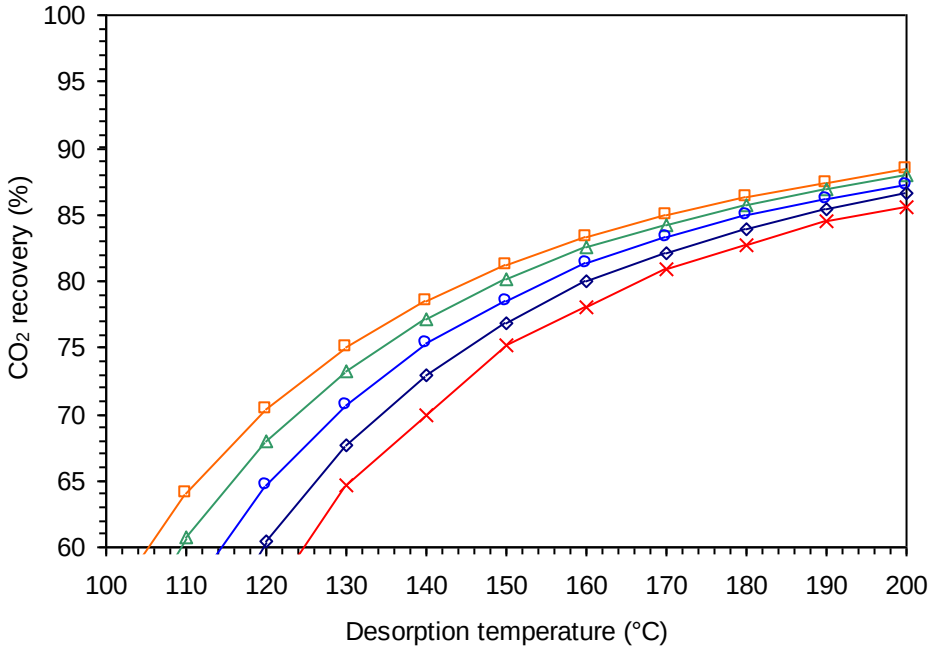
100
95
90
85
80
75
70
65
60
CO2 recovery (%)
100
110
120
130
140
150
160
170
180
190
200
Desorption temperature (°C)

Figure 11

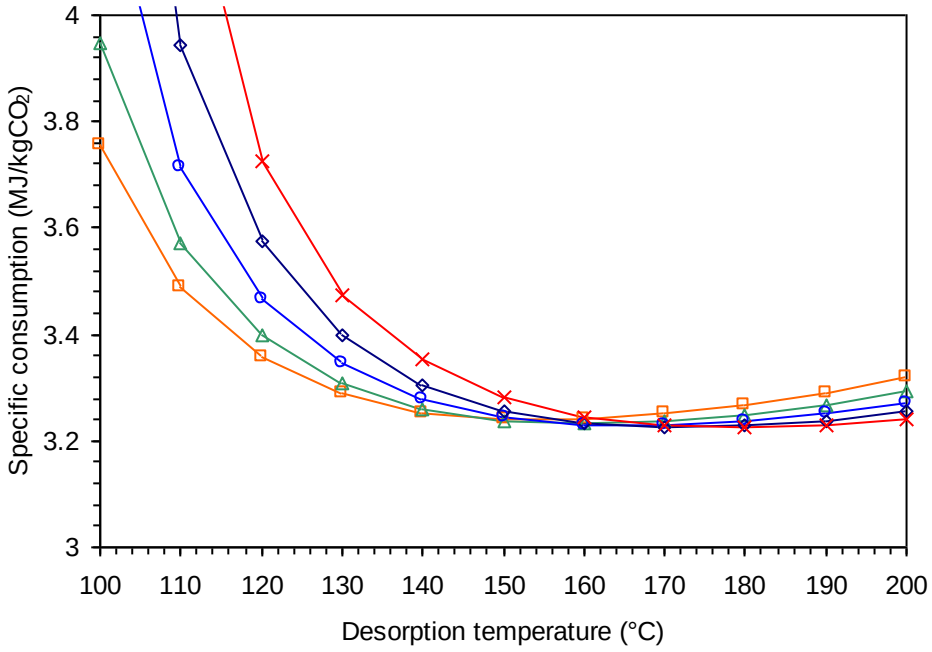
Specific consumption (MJ/kgCO2)
4
3.8
3.6
3.4
3.2
3
100
110
120
130
140
150
160
170
180
190
200
Desorption temperature (°C)

Figure 12